JOURNAL OF COMPUTATIONAL PHYSICS **123,** 341–353 (1996)
ARTICLE NO. 0028

An Impulse-Based Approximation of Fluid Motion due to Boundary Forces

RICARDO CORTEZ

Department of Mathematics and Lawrence Berkeley Laboratory, University of California, Berkeley, California 94720

October 4, 1994; revised June 19, 1995

The motion of an incompressible, inviscid fluid in a region surrounded by a massless, elastic membrane can be approximated by transmitting the effect of the boundary forces to the fluid through vortex dipoles. We present a Lagrangian numerical method for approximating this motion based on the impulse (a.k.a. magnetization) variables introduced by Buttke. In particular, we explain the correspondence between impulse variables and vortex dipoles with a prescribed dipole moment. Numerical examples that illustrate the application of impulse variables in this context are given.

1. INTRODUCTION

There are many interesting situations in which a fluid flows in a region bounded by elastic membranes. Examples of such situations are air flow inside the lungs, blood flow through the heart, and water sloshing inside a balloon. A key feature of these examples is the interaction between the elastic forces that arise on the boundary as the membrane stretches, and the fluid inside. When the fluid is incompressible, these forces immediately affect the motion of the entire fluid; in turn, this motion changes the configuration of the boundary which determines the forces. Our goal is to solve problems with this type of force–fluid interaction.

One approach for the numerical treatment of the interaction between boundary forces and fluid uses the forces to generate vorticity on the boundary and lets the vorticity induce the motion of the fluid (see [20, 19]). Typically the boundary is idealized as infinitely thin. This gives rise to a situation in which forces are singular since they act on a set whose dimension is lower than the spatial dimension of the problem. The singularity of the force field has been a source of instabilities (see [19]). Mendez [20] tracked the motion of an elastic ellipse immersed in an inviscid fluid by introducing pairs of vortex blobs along the boundary to approximate dipoles. The blobs used were of low order and questions regarding changes of the dipole strengths remained unresolved. In the present paper we improve on these ideas by presenting a method which uses higher-order blobs and in which the dipole strengths are updated with the appropriate equation.

McCracken and Peskin [19] applied a vortex-grid hybrid method to the study of blood flow through heart valves. This method made use of a simple vortex layer to introduce the effects of normal boundary forces over each time step and a layer of discrete vortex dipoles to introduce the effects of tangential forces. By a discrete vortex dipole we mean a pair of vortex blobs with equal but opposite strengths a small distance apart.

Our method for introducing the effects of elastic forces on the fluid is based on impulse rather than vorticity. This feature is attractive since the boundary forces naturally interact with the fluid by imparting impulse and these forces are easily accounted for in the method. Furthermore, the use of a discrete approximation of dipoles is no longer necessary because the impulse variables in fact represent dipoles.

Other uses of vortex dipoles or simple vortex layers on free surfaces are found in [2–4, 14, 16, 24]. Baker, Meiron, and Orszag [3, 4] modeled the motion of a periodic free surface between two incompressible, inviscid fluids of different densities using vortex dipoles on the free surface. No surface forces were included in their application. Their method required the formulation of an evolution equation for the dipole strengths which was derived from Bernoulli's equation. The impusle field in our method equals the dipole strength multiplied by a unit vector normal to the surface, and so the equation of motion for impulse updates the dipole strengths appropriately. The problems illustrated in the present paper feature a single fluid (no density jumps) and surface forces. We point out that the methods found in [3, 4, 14, 24] use desingularizing techniques to evaluate the principal value integrals for the velocity at the interface and the vorticity (or dipole) strength. The method adopted here is to use blobs in the discretization of the integrals.

Buttke [7] recently proposed a Lagrangian numerical method for incompressible Euler flow which uses a computational variable that he called velicity. The method is based on the Hamiltonian formulation proposed by Osele-

0021-9991/96 $18.00

dets [21] which is valid in any number of space dimensions. Velicity, the variable conjugate to position, is equal to impulse density for fluids with constant density (see [5, 7]), so here we refer to this computational variable simply as impulse. The same variable is also known as magnetization (e.g., [8, 10]).

In two dimensions the discretization of the impulse field in terms of impulse blobs is equivalent to representing the vorticity in the flow by vortex dipoles with a given dipole moment. This interpretation of impulse allows us to estimate the accuracy with which a given impulse discretization approximates a configuration of vortex pairs; and as a consequence, how this approximation deteriorates in situations when the vortices of a pair drift away from each other. In this paper we explain the equivalence of vortex dipoles and impulse blobs, the relationship between the strength of an impulse vector and the dipole moment, and we illustrate the usefulness of impulse variables by presenting examples in which we compute the motion of a fluid confined to a region with elastic boundary.

In Section 2 we give the definition of impulse density and its relation to the fluid velocity. We also write the equation of motion for impulse and show its consistency with Euler's equations. In Section 3 we present the main ideas of Buttke's method. Section 4 displays the equivalence between discrete impulse in two dimensions and vortex dipoles with a prescribed dipole moment. Section 5 contains the discussion of boundary forces, and Section 6 contains two numerical examples.

2. DEFINITION AND EVOLUTION OF IMPULSE

Consider the incompressible Euler equations in d-dimensional free space (assuming uniform unit density)

$$\mathbf{u}_t + \mathbf{u}\cdot\nabla\mathbf{u} = -\nabla p + \mathbf{F}, \quad \nabla\cdot\mathbf{u} = 0, \tag{1}$$

where $\mathbf{u}$ is the fluid velocity, t is time, $\mathbf{u}_t$ is shorthand notation for $\partial\mathbf{u}/\partial t$, $\nabla\cdot\mathbf{u} = 0$ is the incompressibility condition, p is the pressure, and $\mathbf{F}$ represents external force. We define $\mathbf{m}$ as a vector field equivalent to $\mathbf{u}$ up to a gradient; that is,

$$\mathbf{m} = \mathbf{u} + \nabla\phi. \tag{2}$$

An immediate consequence of Eq. (2) is that the vorticity ξ can be found through $\mathbf{u}$ or $\mathbf{m}$ by $\xi = \nabla\times\mathbf{u} = \nabla\times\mathbf{m}$. Furthermore, for an arbitrary function ϕ, $\mathbf{u}$ is the divergence-free part of the Hodge decomposition (see, e.g., [11]) of $\mathbf{m}$ in free space. The fluid velocity $\mathbf{u}$ is uniquely determined from $\mathbf{m}$ by finding the free-space projection of $\mathbf{m}$ onto the field of divergence-free vectors, denoted by $\mathbf{u} = \mathbb{P}\mathbf{m}$. If the vorticity is confined to a bounded region, then the function ϕ can be chosen to cancel the velocity away from the support of ξ, restricting $\mathbf{m}$ to a set which contains the support of ξ.

Impulse, $\mathbf{I}$, is the total amount of linear momentum required to start the given motion from rest (see [5]). In two dimensions and under the assumption of uniform fluid density ρ, impulse is defined by the equation

$$\mathbf{I} = \rho\int_{\mathbb{R}^2}(y, -x)\,\xi\,d\mathbf{x}.$$

To see that $\mathbf{m}$ is equal to impulse density, assume that $\mathbf{m}$ has compact support, use the definition of impulse, and (2) to obtain (in two dimensions)

$$\begin{aligned}\mathbf{I} &= \rho\int_{\mathbb{R}^2}(y, -x)\,\xi\,d\mathbf{x} = \rho\int_{\mathbb{R}^2}(y, -x)(\partial_x m_2 - \partial_y m_1)\,d\mathbf{x}\\ &= \rho\int_{\mathbb{R}^2}\mathbf{m}\,d\mathbf{x},\end{aligned}$$

where the last equality follows after integration by parts. The same result is true in three dimensions. From this point on, we refer to $\mathbf{m}$ as impulse.

The evolution equation for $\mathbf{m}$ can be derived using Eq. (2) and the identities:

(ID1) $\nabla(\frac{1}{2}|\mathbf{u}|^2) = (\nabla\mathbf{u})^{\mathrm{T}}\mathbf{u}$,

(ID2) $(D/Dt)\nabla\phi = \nabla(D\phi/Dt) - (\nabla\mathbf{u})^{\mathrm{T}}\nabla\phi$,

where $\nabla\mathbf{u}$ is a matrix with entries $(\nabla\mathbf{u})_{ij} = \partial u_i/\partial x_j$, T denotes the transpose, and $D/Dt = \partial_t + \mathbf{u}\cdot\nabla$ is the material derivative. Solving for $\mathbf{u}$ in Eq. (2) we write

$$\begin{aligned}\frac{D\mathbf{u}}{Dt} + \nabla p &= \frac{D\mathbf{m}}{Dt} - \frac{D}{Dt}\nabla\phi + \nabla p\\ &= \frac{D\mathbf{m}}{Dt} + (\nabla\mathbf{u})^{\mathrm{T}}\mathbf{m} - \nabla\left(\frac{D\phi}{Dt} + \frac{1}{2}|\mathbf{u}|^2 - p\right).\end{aligned}$$

It is easy to see that if $\mathbf{u} = \nabla\chi$, where $\chi = -\phi$, then $\nabla(D\phi/Dt + \frac{1}{2}|\mathbf{u}|^2 - p) = 0$ from Bernoulli's equation. This serves as motivation for letting $\mathbf{m}$ evolve according to

$$\mathbf{m}_t + \mathbf{u}\cdot\nabla\mathbf{m} = -(\nabla\mathbf{u})^{\mathrm{T}}\mathbf{m} + \mathbf{F}. \tag{3}$$

For a derivation of the continuous Hamiltonian formulation of incompressible fluid flow using impulse variables, see [18, 17, 21]. We remark that in the case of viscous fluid with viscosity ν, the equations of motion for impulse, Eq. (3), are replaced by (see [7, 12])

$$\mathbf{m}_t + \mathbf{u}\cdot\nabla\mathbf{m} = -(\nabla\mathbf{u})^{\mathrm{T}}\mathbf{m} + \nu\Delta\mathbf{m} + \mathbf{F}. \tag{4}$$

3. THE NUMERICAL METHOD IN TWO DIMENSIONS

A Lagrangian numerical method based on impulse can be outlined in the following way: (1) approximate the im-

pulse field by some discretization, (2) find $\mathbf{u}$ from $\mathbf{m}$ via a projection, (3) advance the particles and update the impulse strengths.

3.1. *The Approximate Impulse Field*

Let $\mathbf{m}(\mathbf{x})$ represent the exact impulse field. Following Buttke [7], we approximate $\mathbf{m}(\mathbf{x})$ by a collection of impulse blobs $\tilde{\mathbf{m}}(\mathbf{x}) = \sum \mathbf{m}^j f_\delta(\mathbf{x} - \mathbf{x}^j)$ centered at locations $\mathbf{x}^j$. The impulse strengths $\mathbf{m}^j$ are initially set equal to $\mathbf{m}(\mathbf{x}^j)$ multiplied by an area element. The cutoff function f_δ is a smooth approximation to the delta function and, as in a vortex method, is chosen to satisfy certain conditions for the purpose of accuracy. In particular, $f_\delta(\mathbf{x}) = \delta^{-2} f_1(\mathbf{x}/\delta)$, where the cutoff radius δ is a small but fixed parameter and f_1 is a smooth function satisfying:

1. $\int f_1(\mathbf{x})\, d\mathbf{x} = 1$
2. $\int \mathbf{x}^\alpha f_1(\mathbf{x})\, d\mathbf{x} = 0,\ 0 < |\alpha| < k$
3. $\int \mathbf{x}^\alpha f_1(\mathbf{x})\, d\mathbf{x} < \infty,\ |\alpha| = k.$

Here α is a two-dimensional multiindex and k is a fixed positive integer. A function satisfying the conditions outlined above is referred to as a kth-order cutoff function because in the context of vortex methods, the replacement of the vorticity $\xi(\mathbf{x})$ by $\int \xi(\mathbf{y}) f_\delta(\mathbf{x} - \mathbf{y})\, d\mathbf{y}$ causes changes in the velocity field which are $O(\delta^k)$. For a detailed analysis of cutoff functions see [6]. In this paper we use the radially symmetric function $f_1(r) = (1/2\pi)(e^{-r^2} + \frac{1}{2}e^{-r^2/2})$ of order 2. The appropriateness of adopting cutoff functions from vortex theory into impulse methods is discussed in Section 4.

3.2. *The Particle Velocities Due to Impulse*

In order to update the impulse particle positions, we must compute the velocity at each particle location. The projection, the process of finding the velocity $\mathbf{u}$ in terms of $\mathbf{m}$, can be done exactly for a good choice of radially symmetric function f_δ. This is done as follows:

1. The velocity field $\mathbf{u}$ is related to impulse by an approximation of Eq. (2); namely $\tilde{\mathbf{m}} = \mathbf{u} + \nabla\phi$, for some ϕ. Take the divergence of this equation to obtain

$$\Delta\phi = \nabla \cdot \tilde{\mathbf{m}} = \sum \mathbf{m}^j \cdot \nabla f_\delta(\mathbf{x} - \mathbf{x}^j).$$

Suppose that a function ψ satisfies $\Delta\psi = f_\delta$, then we could write $\phi = \sum \mathbf{m}^j \cdot \nabla\psi$. This observation is important because ψ does not depend on the flow and so ψ can be found once and for all.

2. Since f_δ is radially symmetric, the equation for ψ can be written in polar coordinates

$$\frac{1}{r}(r\psi_r)_r = f_\delta(r),$$

where the subscript r represents a partial derivative with respect to r. Ultimately we only need the gradient of ψ, not ψ itself, so we solve the last equation for ψ_r and obtain

$$\psi_r(r) = \frac{1}{r}\int_0^r q f_\delta(q)\, dq = \frac{1}{2\pi r} F(r),$$

where $F(r) = \int_{|\mathbf{x}|\le r} f_\delta(|\mathbf{x}|)\, d\mathbf{x}$ is called the shape factor and depends only on the cutoff function.

3. We can now find an expression for ϕ, which we differentiate to find $\nabla\phi$ and finally let $\mathbf{u} = \tilde{\mathbf{m}} - \nabla\phi$. The final result in terms of the shape factor is

$$\begin{aligned}\mathbf{u}(\mathbf{x}) = \sum \mathbf{m}^j &\left[\frac{rF'(r) - F(r)}{2\pi r^2}\right] \\ &- \hat{\mathbf{x}}^j(\mathbf{m}^j \cdot \hat{\mathbf{x}}^j)\left[\frac{rF'(r) - 2F(r)}{2\pi r^2}\right],\end{aligned} \tag{5}$$

where $\hat{\mathbf{x}}^j = (\mathbf{x} - \mathbf{x}^j)/r$ and $r = |\mathbf{x} - \mathbf{x}^j|$.

The particle positions are advanced using $d\mathbf{x}^j/dt = \mathbf{u}(\mathbf{x}^j)$.

3.3. *The Update of Impulse Strengths*

The impulse strengths must be updated with an equation approximating Eq. (3). To this end we differentiate the expression for $\mathbf{u}$ to obtain the matrix $\nabla\mathbf{u}$, and we calculate any forces at $\mathbf{x}^j$. The impulse strengths are updated using $d\mathbf{m}^j/dt = -(\nabla\mathbf{u})^{\mathrm{T}}\mathbf{m}^j + \mathbf{f}^j$, where $\mathbf{f}^j$ is the force on the piece of boundary represented by the jth particle (see Section 5).

In summary the algorithm looks like this:

1. Given $\tilde{\mathbf{m}}(\mathbf{x}) = \sum \mathbf{m}^j f_\delta(\mathbf{x} - \mathbf{x}^j)$, find expressions for $\mathbf{u}(\mathbf{x}) = \mathbb{P}\tilde{\mathbf{m}}$ and $\nabla\mathbf{u}$.

2. Update the particle positions and impulse strengths with

$$\frac{d\mathbf{x}^j}{dt} = \mathbf{u}(\mathbf{x}^j) \tag{6}$$

$$\frac{d\mathbf{m}^j}{dt} = -(\nabla\mathbf{u})^{\mathrm{T}}\mathbf{m}^j + \mathbf{f}^j. \tag{7}$$

4. IMPULSE AND VORTICITY IN TWO DIMENSIONS

In this section we explain the connection between a collection of impulse blobs and a collection of vortex dipoles. This connection leads to the conclusion that a discrete vortex dipole (two vortex blobs a small distance apart) induces a velocity field which is a centered-difference approximation of the velocity field induced by an impulse blob which uses the same cutoff function. This observation allows us to import into the analysis of the

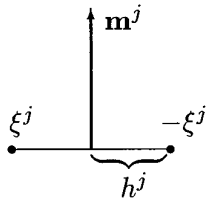

FIG. 1. Vortex pair approximation to impulse vector.

impulse method the role of the cutoff function in the accuracy of vortex methods.

A collection of impulse blobs, $\tilde{\mathbf{m}}(\mathbf{x}) = \sum_j \mathbf{m}^j f_\delta(\mathbf{x} - \mathbf{x}^j)$, immediately defines the vorticity in the flow. Since $\xi = \nabla \times \tilde{\mathbf{m}}$, we have

$$\xi(\mathbf{x}) = \sum_j \nabla f_\delta(\mathbf{x} - \mathbf{x}^j) \cdot (\mathbf{m}^j \times \hat{\mathbf{z}}),$$

where $\hat{\mathbf{z}}$ is the unit vector normal to the plane. Each term in the sum is $|\mathbf{m}^j|$ multiplied by the derivative of f_δ in the direction of $(\mathbf{m}^j \times \hat{\mathbf{z}})$. Let $\mathbf{h}^j$ be a vector of magnitude h^j in the direction of $(\mathbf{m}^j \times \hat{\mathbf{z}})$ (see Fig. 1) and write the derivative of f_δ in the direction of $\mathbf{h}^j$ as

$$\begin{aligned}\xi(\mathbf{x}) &= \sum_j |\mathbf{m}^j| \lim_{h^j \to 0} \frac{f_\delta(\mathbf{x} + \mathbf{h}^j - \mathbf{x}^j) - f_\delta(\mathbf{x} - \mathbf{h}^j - \mathbf{x}^j)}{2h^j} \\ &= \sum_j \lim_{h^j \to 0} \xi^j [f_\delta(\mathbf{x} + \mathbf{h}^j - \mathbf{x}^j) - f_\delta(\mathbf{x} - \mathbf{h}^j - \mathbf{x}^j)],\end{aligned} \tag{8}$$

where the vortex strenths ξ^j are found with the formula $\xi^j = |\mathbf{m}^j|/2h^j$. Expression (8) shows that the vorticity induced by the collection of impulse blobs is exactly the vorticity generated by a collection of smoothed vortex dipoles. Each dipole is the limit of two vortex blobs of equal but opposite strength as their separation vanishes; the limit is taken in a way that keeps the vortex dipole moment equal to $\hat{\mathbf{z}} \times \mathbf{m}^j$.

Note that an impulse blob is equivalent to a smoothed vortex dipole which uses the same cutoff function as impulse. This function provides the smoothing to approximate the Biot–Savart integral with high accuracy. This analysis validates the use of vortex cutoff functions in impulse methods and shows that the relationship between the cutoff radius and the initial particle separation needed for the convergence of vortex methods must be respected. This relationship is typically of the form $\delta = h^q$, where h is the particle separation and q is a number such that $0 < q < 1$ (see [1, 6, 13]). If impulse is defined along a curve and is normal to it, we can write $\mathbf{m}$ in local coordinates (s, n) (tangent and normal to the curve, respectively) as $(0, m_n)$. Then the relation $\xi = \nabla \times \mathbf{m}$ implies that the vortex sheet strength is the tangential derivative of the component of impulse normal to the curve. Thus the dipole strength is the magnitude of the impulse vector with sign determined by the direction of impulse relative to the unit normal.

Boundary forces naturally interact with the fluid by imparting impulse. The impulse blobs of our numerical method are precisely what is needed to introduce the effect of forces on the fluid by the use of vortex dipoles, since impulse blobs are vortex dipoles. Furthermore, our method includes equations for the evolution of the dipole strengths. Previous methods did not include an adequate system for updating dipole strengths and used vortex pairs to approximate dipoles which introduced an additional error, corresponding to the centered-difference approximation of the derivative in (8).

The velocity at an arbitrary point $\mathbf{x}$ due to a collection of impulse blobs is given by Eq. (5)

$$\begin{aligned}\mathbf{u}(\mathbf{x}) = \sum \mathbf{m}^j &\left[\frac{rF'(r) - F(r)}{2\pi r^2}\right] \\ &- \hat{\mathbf{x}}^j(\mathbf{m}^j \cdot \hat{\mathbf{x}}^j)\left[\frac{rF'(r) - 2\mathrm{F}(r)}{2\pi r^2}\right].\end{aligned}$$

This equation can be manipulated to look like

$$\mathbf{u}(\mathbf{x}) = [D\mathbf{K}_\delta(\mathbf{x})](\mathbf{m} \times \hat{\mathbf{z}}), \tag{9}$$

where $\mathbf{K}_\delta(\mathbf{x}) = (-y, x)^{\mathrm{T}} F(r)/2\pi r^2$is the kernel of the vortex method. The derivative in (9) is the result of taking the limit of the velocity field due to two vortex blobs as their separation vanishes while maintaining a constant dipole moment.

It is important to point out that a collection of impulse variables that initially induces vorticity, given by a collection of vortex blobs, may later evolve into a configuration of impulse vectors whose induced vorticity no longer approximates the evolved vortices with the same accuracy. For a detailed description of how this happens and of ways to prevent accuracy loss of the impulse discretization see Cortez [12]. This type of accuracy loss is not present in the examples discussed in this paper.

5. BOUNDARY FORCES

The forces exerted by an elastic membrane on the fluid are given by (see [19])

$$\mathbf{F}(\mathbf{x}) = \int \mathbf{f}(s)\delta(\mathbf{x} - \mathbf{x}(s))\, ds, \tag{10}$$

where s is the arclength parameter, $\mathbf{x}(s)$ is a parametrization of the boundary, $\mathbf{f}$ is the force density, and δ is the two-dimensional Dirac delta function. Note that $\mathbf{F}$ is singu-

lar since the integral is taken along a curve and δ is two-dimensional.

The force density is of the form $\mathbf{f}(s) = d(T\hat{\tau})/ds$, where T is tension and $\hat{\tau}$ is the unit vector tangent to the boundary (see [22]). We apply the product rule to the definition of force density to get

$$\mathbf{f}(s) = \frac{d(T\hat{\tau})}{ds} = \frac{dT}{ds}\hat{\tau} + T\frac{d\hat{\tau}}{ds} = \frac{dT}{ds}\hat{\tau} + T\kappa\hat{n}, \qquad (11)$$

where κ is the curvature and $\hat{n}$ is the outward unit vector normal to the boundary. Since in Euler flow tangential forces will simply make the boundary slip and not affect the fluid, we conclude that $\mathbf{f}$ must be in the direction normal to the boundary and $dT/ds = 0$ along the membrane at any moment in time. We emphasize that the tension is not constant in time. The forces are then found from the equation

$$\mathbf{f}(s) = T\kappa\hat{n}. \qquad (12)$$

In practice, the forces are found at points on the boundary where impulse vectors are located. Each force vector is associated with a piece of arclength corresponding to the discretization of the boundary. Equation (10) is discretized by

$$\mathbf{F}(\mathbf{x}) = \sum_j \mathbf{f}^j f_\delta(\mathbf{x} - \mathbf{x}^j),$$

where $\mathbf{f}^j = \mathbf{f}(\mathbf{x}^j)h^j(t)$ and $h^j(t)$ is the discretization size of the jth particle. Each piece of arclength (the discretization size) is thought of as a rubber band with a stiffness constant and a rest-length. Denote by h_0^j the rest-length corresponding to $h^j(t)$, then the tension at $\mathbf{x}^j$ is defined by the equation

$$T(\mathbf{x}^j) = \begin{cases} \sigma(h^j(t) - h_0^j)/h_0^j, & h^j(t) > h_0^j, \\ 0, & h^j(t) \le h_0^j, \end{cases}$$

where σ is a stiffness constant. We will only consider the case when all h_0^j are equal.

For inviscid flow, the tension must be constant along the membrane at any instant in time. To enforce this condition for equal h_0^j, the boundary points $\mathbf{x}^j$ must be equally distributed at the end of every time step. This is accomplished by placing a cubic polynomial between two consecutive boundary points matching the slope of the line tangent to the membrane at those points and by moving one of the points along this curve to the appropriate location. The initial point in this process is chosen arbitrarily.

The curvature in Eq. (12) is also found using a cubic polynomial to interpolate the boundary. This time the polynomial is chosen to match the location of three adjacent points and the slope of the line tangent to the membrane at the middle point. The curvature at the middle point is approximated by the curvature of the polynomial. No additional work is required to find the slopes of the tangent lines since the impulse vectors are known to be normal to the membrane at all times.

6. NUMERICAL EXAMPLES

In this section we present two numerical examples of the motion of a massless, elastic membrane immersed in an incompressible, inviscid fluid. The membrane is assumed to move with the local fluid velocity and to be initially under tension. We begin with a few comments on the time-stepping procedure.

6.1. *Time Stepping*

At each time step we must update the particle positions and the impulse vectors as described by Eqs. (6) and (7). We use the following time-splitting procedure:

1. Since $\mathbf{f}^j$ is a rate of change of impulse, $\Delta t\ \mathbf{f}^j$ is the impulse imparted by a constant force $\mathbf{f}^j$ during one time step Δt. Given the current impulse vectors and particle positions, add the effect of the forces at the beginning of the time step:

$$\mathbf{m}^j \leftarrow \mathbf{m}^j + \Delta t\mathbf{f}^j. \qquad (13)$$

2. Update the positions and impulse strengths:

$$\frac{d\mathbf{x}^j}{dt} = \mathbf{u}(\mathbf{x}^j) \qquad (14)$$

$$\frac{d\mathbf{m}^j}{dt} = -(\nabla\mathbf{u})^{\mathrm{T}}\mathbf{m}^j. \qquad (15)$$

The unit normal vectors needed to add the effect of the forces are found by updating and normalizing vectors initially perpendicular to the boundary. Vectors normal to the boundary which are evolved using Eq. (15) remain normal to the boundary [12].

A Runge–Kutta method of order 5 was used to solve Eqs. (14)–(15). The numerical results were compared with results from an iterative method in which the configuration at the end of the time step was the one used to calculate the forces acting during that step. This comparison showed no significant differences and so we opted to use the procedure described above for its simplicity.

6.2. *Example* 1: *An Ellipse Moving under Tension*

The first example begins with the membrane in the shape of the ellipse $(3x/2)^2 + y^2 = 1$ (see Fig. 2). This curve was discretized with 240 equally spaced points yielding a discretization size $h = 2.204 \times 10^{-2}$. The rest-length of all

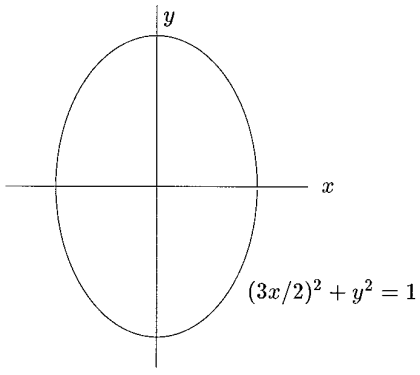

FIG. 2. Initial configuration for Example 1.

elements was set to half the initial discretization size, and the stiffness σ was set to $\frac{1}{2}$. The cutoff radius δ (for f_δ) was fixed at 0.12.

The motion of the membrane as it goes through one cycle (from vertical to horizontal and back) is depicted in Fig. 3. Although the membrane appears to return to its initial configuration, there is no confirmation that the motion is periodic, starting from the given initial conditions. One might ask the question: is the membrane elliptical for $t > 0$? The eccentricity of ellipses of constant area defines their arclength. The graph of eccentricity versus arclength for ellipses of area equal to the area enclosed by the initial membrane is shown as a solid line in Fig. 4. The eccentricity of an ellipse is defined as $[1 - (a/b)^2]^{1/2}$, where a and b are the minor and major axes, respectively. If we assume that the membrane remains elliptical for all time, its eccentricity can be calculated at every step and plotted against the arclength. At time $t = 0$ the ellipse corresponds to the point labeled A in Fig. 4. As the membrane moves and becomes circular the eccentricity decreases to zero (point B) and then increases back to point A when the membrane becomes elongated horizontally. The plot moves back to point B and finally back to point A to complete one cycle. The results for $0 \le t \le 4.48$ shown in Fig. 4 and the convexity of the region inside the membrane validate our assumption. We conclude from the figure that the membrane is approximately elliptical during the motion.

We now present numerical evidence of the convergence of the method. Each particle used to represent the boundary is associated with a piece of the membrane whose length we call the discretization size. Suppose the initial discretization size is h (corresponding to N particles) and the solution is found up to a time $T > 0$. We then solve the problem again with $h/2$ as the discretization size (corresponding to $2N$ particles) and compare the positions of the N particles in the first run with the positions of the corresponding particles in the second run; that is, those particles which have the same initial positions as the original N particles. We define the error $e(\mathbf{x}_N, \mathbf{x}_{2N})$ to be the maximum of the distances between corresponding particles. The ellipse problem was solved up to time $T = 5.76$ using $\Delta t = 0.16$ and 0.08, as well as three levels of refinement of the discretization size, those corresponding to 120, 240, and 480 particles. The maximum distance between the 120 particles common to all runs was calculated at times $t = 3.2$, 4.48, and 5.76. These times yield results that are representative of the entire motion. The results, Tables I and II, show that as the time step decreases, the errors also decrease. It is also evident from the tables that for a small enough time step, the errors decrease by about a factor of 4 when the discretization size is halved, indicating second-order convergence. This reflects the fact that the midpoint rule is being used to approximate the line integral needed to compute the forces along the membrane.

Throughout the motion of the membrane, two quantities that must remain invariant are the area inside the membrane and the total energy. Since the fluid is incompressible, the area of the region bounded by the membrane must remain constant in time. In addition, the kinetic energy of the fluid must balance the changes in the elastic energy of the membrane. Thus, another invariant of the motion is the total energy: kinetic plus elastic.

The kinetic energy, is given by $KE = 1/2 \sum \mathbf{m}^j \cdot \mathbf{u}(\mathbf{x}^j)$ (see [7]), while the elastic energy is $EE = (\sigma/2) \sum (h^j(t) - h_0^j)^2/h_0^j$, when $h^j(t) > h_0^j$, and zero otherwise. Note that the kinetic energy depends explicitly on the cutoff function f_δ since $\mathbf{u}$ does. The approximate conservation of area and energy over a period of time long enough for the membrane to go through more than two cycles is shown in Fig. 5. At $t = 10$, both quantities are still conserved to within 0.5% of their initial values (for $\Delta t = 0.008$, $\delta = 0.12$, and $h = 2.204 \times 10^{-2}$). We found that the relative deviation of area and total energy from their initial values was proportional to the time step. The slight changes of these invariants are a consequence of the interpolation procedures during the redistribution of points on the boundary and can be reduced by the use of better interpolation methods. In problems where interpolation is not required, the solution of the Hamiltonian system (6)–(7) (for $\mathbf{f}^j \equiv 0$) with Runge–Kutta methods has been shown to conserve area and kinetic energy to an accuracy of 1×10^{-7} with comparable time steps [7].

The effect of different cutoff radii was studied by solving the problem using several values of δ. The membrane was first discretized using 480 particles corresponding to a discretization size of $h = 1.102 \times 10^{-2}$. The motion of the ellipse shown in Fig. 3 is representative of the motions observed for various values of δ between 0.02 and 0.12. The main observation is that the period of the motion is sensitive to the choice of cutoff radius as illustrated in Fig. 6. The periods shown in the figure were computed based on the local maximum of the eccentricity. As δ decreases,

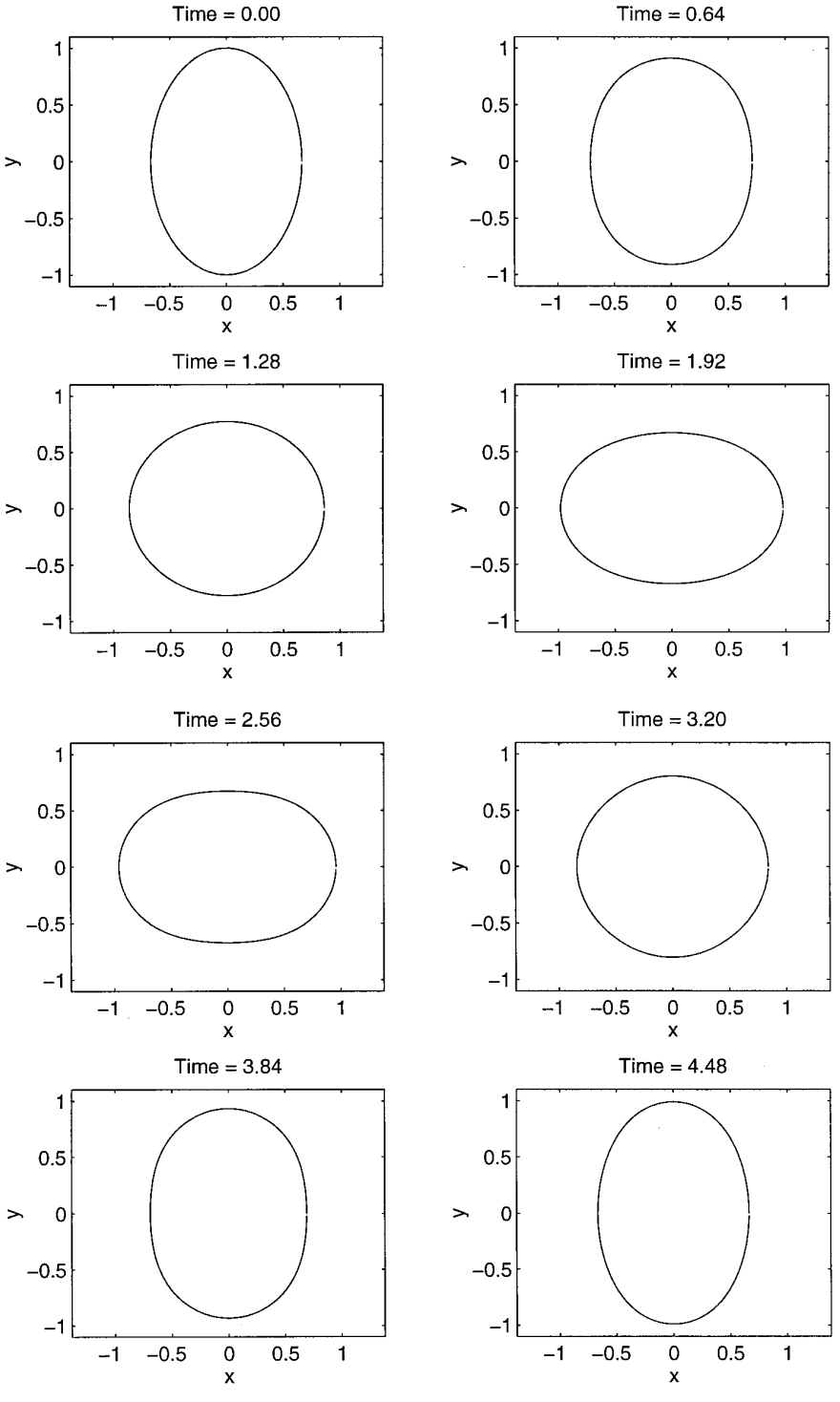

FIG. 3. Motion of the membrane of example 1 for time t = 0 − 4.48 with $\Delta t = 0.008$.

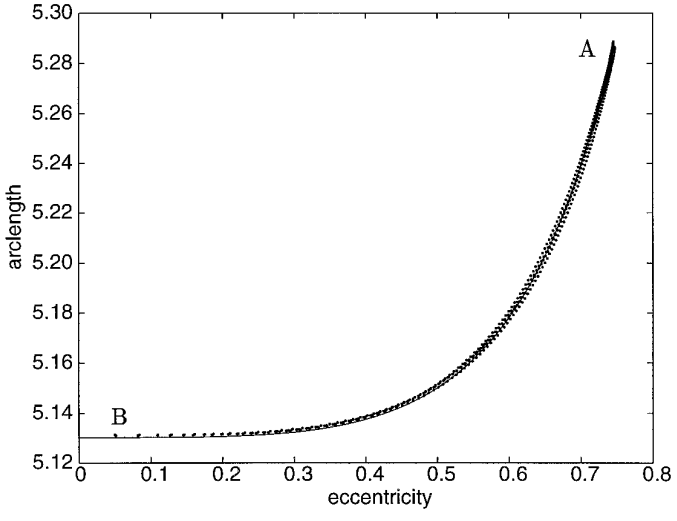

FIG. 4. Eccentricity versus arclength. The solid line is the graph for ellipses of fixed area equal to the initial area enclosed by the membrane; the dots are points obtained for the motion of the membrane in Example 1.

the velocities induced at a point by nearby particles are larger and the result is a shorter period. The figure indicates that as $\delta \to 0$ the period converges to some p_0. Assuming the period p satisfies $p = p_0 + C\delta^\gamma$ and using the three left-most points, we can extrapolate the data to find $p_0 \approx 4.018$.

6.3. *Example* 2: *A Nonconvex Membrane*

The initial setup for the second example consists of a membrane in a shape that simulates a water balloon being poked with a finger (see Fig. 7). When we remove the finger, the strong forces on the indented part of the boundary make this portion move faster than the rest, creating waves which propagate along the boundary. The exact shape of the initial membrane is given in polar coordinates by $x(\theta) = r(\theta)\cos(\theta)$ and $y(\theta) = r(\theta)\sin(\theta)$, where $r(\theta) = 1 - \frac{7}{10}(1 - 10q^3 + 15q^4 - 6q^5)$, $q = 2\theta/\pi$ on the right half plane, and $r(\theta) = 1$ on the left half plane.

The boundary was discretized using 300 equally spaced particles for a discretization size of $h = 1.92 \times 10^{-2}$ and the rest-length of all elements was set to half the initial discretization size. The stiffness σ was set to $\frac{1}{2}$ for all elements and the cutoff radius δ was fixed at 0.12.

TABLE I

Errors for $\Delta t = 0.16$ at $t = 3.2$, 4.48, and 5.76

	$\Delta t = 0.16$		
	$t = 3.20$	$t = 4.48$	$t = 5.76$
$e(\mathbf{x}_{120}, \mathbf{x}_{240})$	0.5338E-3	0.7033E-3	1.651E-3
$e(\mathbf{x}_{240}, \mathbf{x}_{480})$	0.2006E-3	0.2750E-3	0.5631E-3
Error ratio	2.66	2.56	2.93

TABLE II

Errors for $\Delta t = 0.08$ at $t = 3.2$, 4.48, and 5.76

	$\Delta t = 0.08$		
	$t = 3.20$	$t = 4.48$	$t = 5.76$
$e(\mathbf{x}_{120}, \mathbf{x}_{240})$	0.4427E-3	0.3032E-3	1.0943E-3
$e(\mathbf{x}_{240}, \mathbf{x}_{480})$	0.1084E-3	0.0743E-3	0.2633E-3
Error ratio	4.08	4.08	4.16

The motion of the membrane for time 0 through 5.4 and $\Delta t = 0.004$ is seen in Figs. 8 and 9. In this example, as well as the first one, the initial impulse field was identically zero. It is the forces created by the initial membrane configuration that get the motion started by introducing impulse along the membrane. Of the two invariants, the energy is typically more sensitive than the area to the boundary treatment. In this example the energy was conserved to within 4% of its initial value and area to within 0.5% of its initial value for times up to 5.4.

In Fig. 8 one can detect waves propagating along the boundary from right to left. These get started when the initially indented portion of the boundary moves out. The first frame of Fig. 9 shows the waves beginning to travel back and new waves forming as the left side of the membrane slightly vibrates. These new waves have frequency components essentially of the same size as the original wave. We observe that while the waves are on one side of the membrane, the other side remains fairly smooth and circular. This smoothness gets disturbed only when several waves have formed and interacted with one another. By then, the radial distance to the smooth part of the boundary slightly oscillates around a constant value.

Since the forces are normal to the boundary, the impulse field at the beginning of each time step is also normal to the

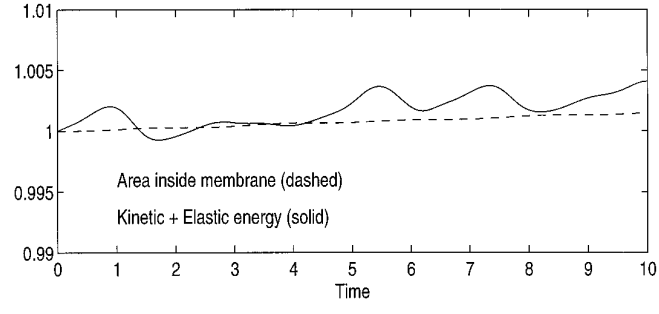

FIG. 5. Relative change of invariants of Example 1 for 240 particles and $\Delta t = 0.008$.

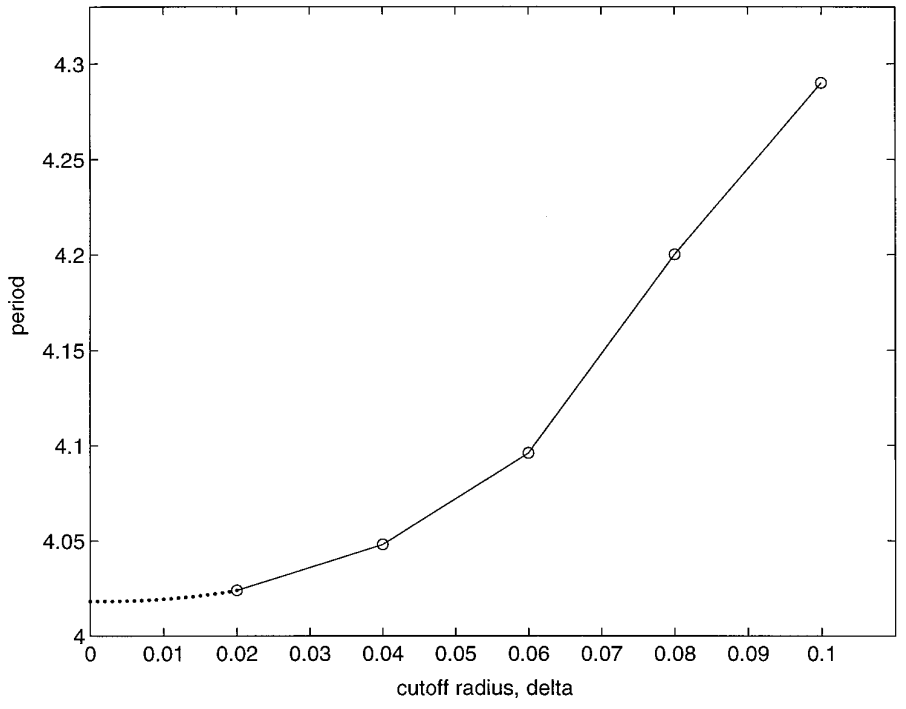

FIG. 6. Variation of period of the ellipse as a function of cutoff radius δ. Data for $h = 1.102 \times 10^{-2}$ and $\Delta t = 0.008$.

boundary. As $\tilde{\mathbf{m}}$ evolves with Eq. (15), it remains normal to the boundary (see [12]). Figure 10 shows the impulse field at times $t = 1.2$ and $t = 5.0$. For clarity, the vectors have been scaled by a factor of 2 and only every other vector is shown. The forces on the right side of the membrane point outward during a short, initial time interval. This causes the impulse vectors to grow outwardly first and then to shrink gradually and reverse their direction as that portion of the membrane becomes convex. The top of Fig. 10 shows some vectors are still in this process (more detail has been added to this portion of the figure). Since force is a rate of change of impulse, the impulse field at any time represents the accumulation of forces up to that time. As a consequence, the size of the impulse vectors generally increases in time (since most of the time, force on any piece of boundary points inward) even though the discretization size stays near but below its initial value. The growth of the impulse vectors is observed in Fig. 10.

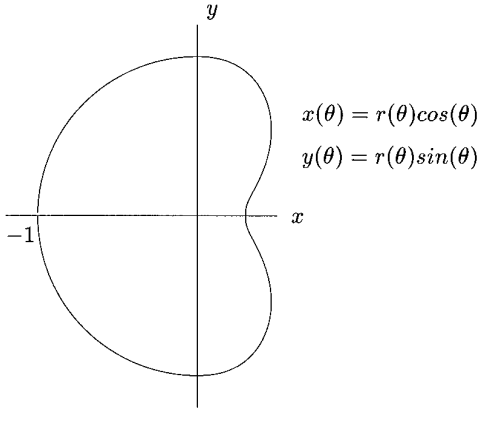

FIG. 7. Initial membrane configuration of Example 2.

7. CONCLUSIONS

We have shown that the approximation of the impulse field in two dimensions is equivalent to approximating the vorticity in the flow with vortex dipoles. We have also shown the connection between the strength of an impulse blob and the vortex dipole moment. The equation of motion for impulse automatically evolves the strengths of the dipoles. A numerical method for the incompressible Euler equations based on impulse was applied to problems in which a fluid is surrounded by an elastic membrane. The calculations show evidence of the convergence of the method. Two attractive features of the method are that the treatment of forces is simple and that it preserves well at least two invariants of the flow: the area inside the membrane and the total energy. Of course, the simple nature of the treatment of the boundary forces is a result of the assumption that the forces are constant during each time step, and thus their impulse can simply be added to the existing impulse at the beginning of each step. Since

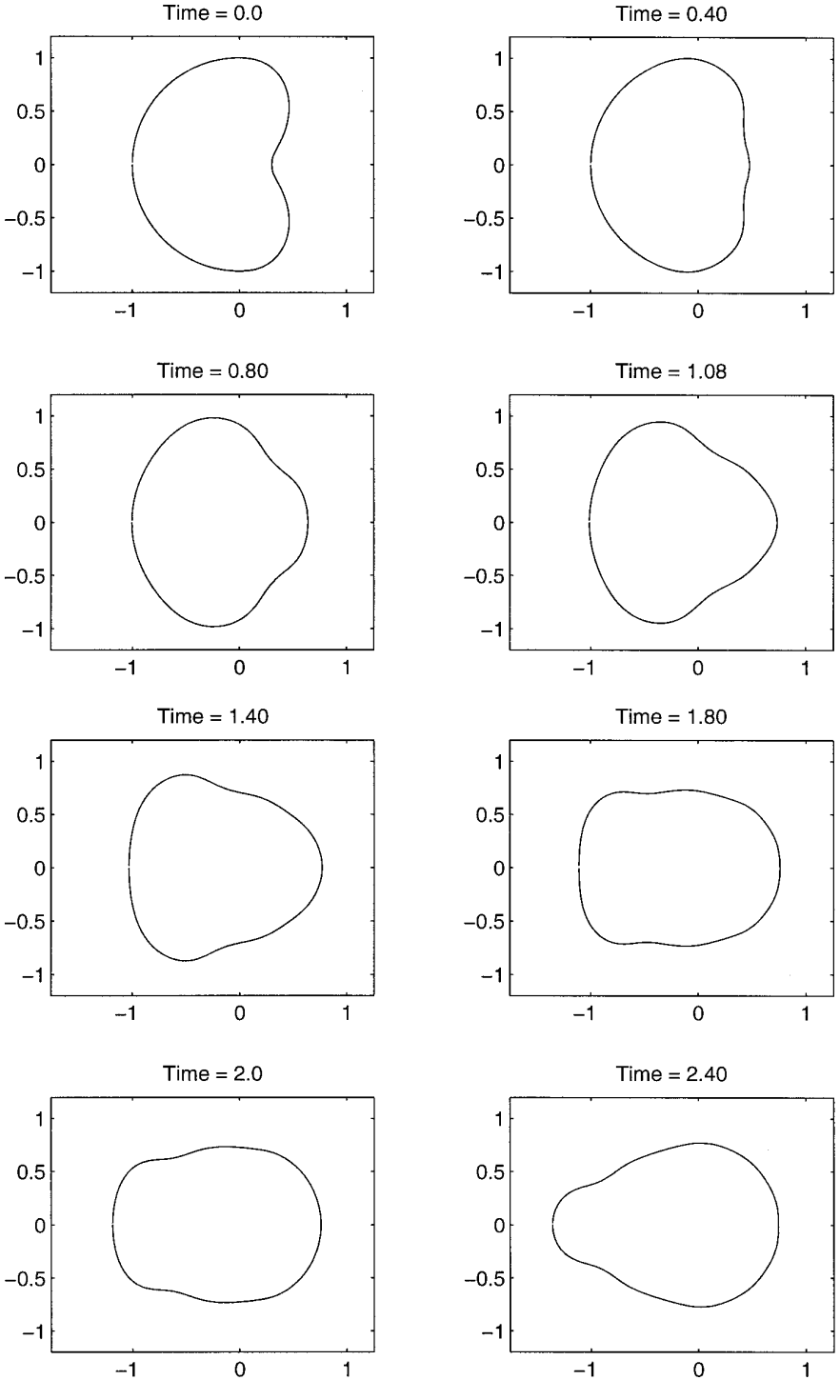

FIG. 8. Motion of the membrane of Example 2 for time $t = 0 - 2.4$ with $\Delta t = 0.004$.

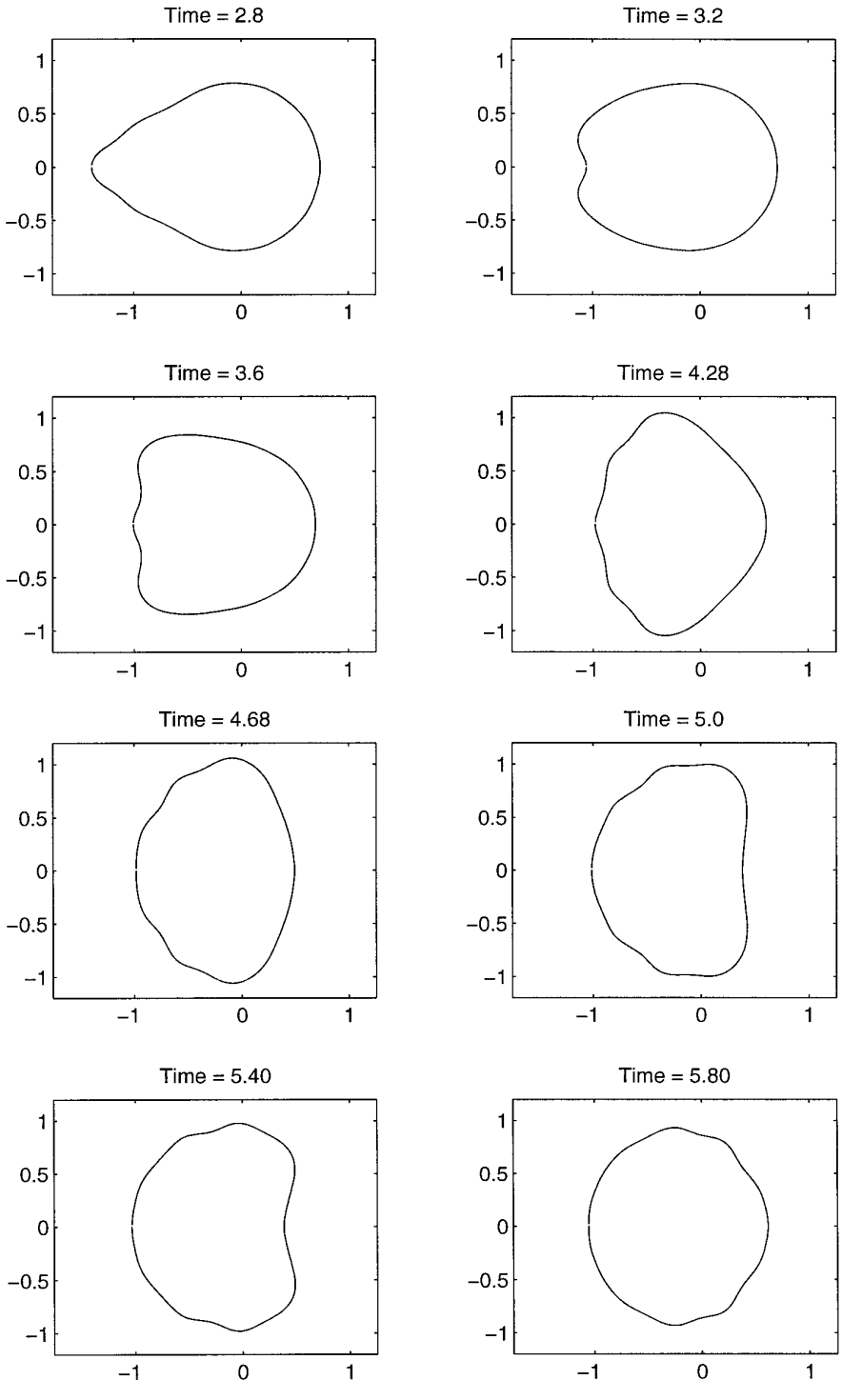

FIG. 9. Motion of the membrane of Example 2 for time $t = 2.8 - 5.8$, with $\Delta t = 0.004$.

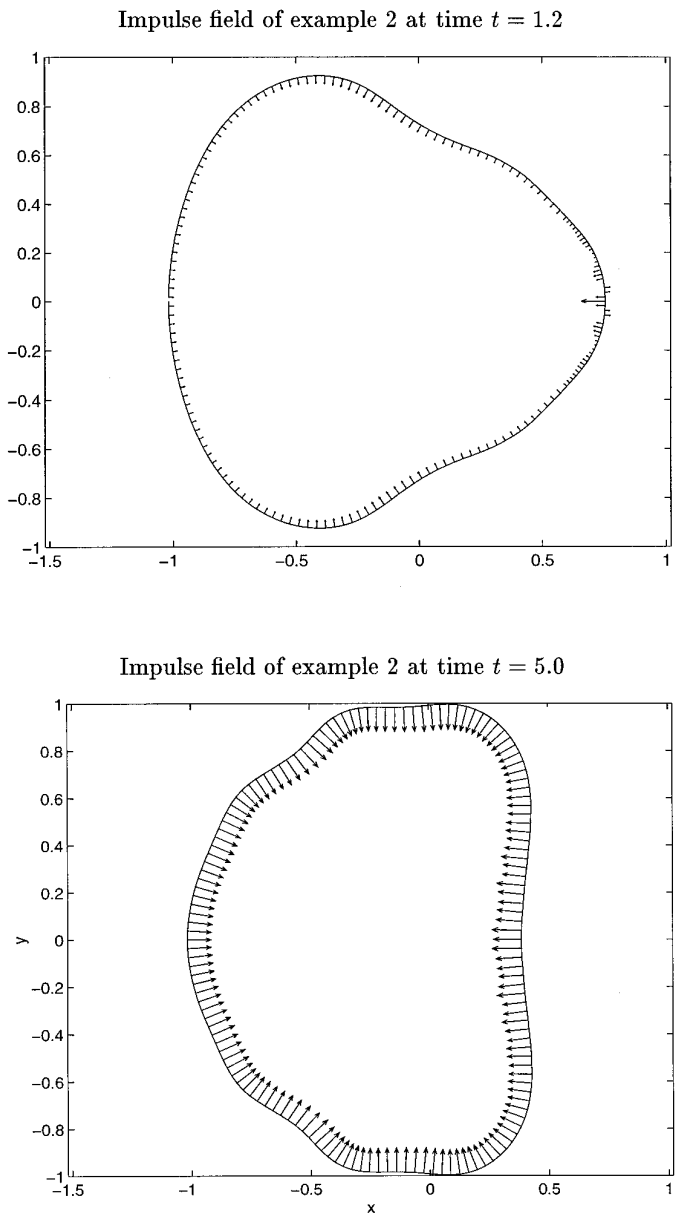

FIG. 10. Impulse field of Example 2 at times $t = 1.2$ and $t = 5.0$.

the forces are proportional to the local curvature of the membrane, high curvatures will produce strong forces, which in turn will require a reduction of the time step until the configuration of the boundary allows the return to larger steps.

We expect this method to be useful in approximating flow in regions with more complicated geometries, such as the interior of the human heart, and in situations that account for vicous effects and include physical constraints. A physical constraint may be a piece of the membrane which is fixed in space; more general geometrical considerations might include portions of the boundary with corners or cusps. The treatment of such constraints requires a mechanism which does not rely on curvature for computing forces along singular portions of the boundary, since curvature is infinite there. This feature is not part of the current implementation of the method and will be the focus of future work.

The effect of viscosity can be introduced in a straightforward manner as in vortex methods. The algorithm for the viscous case is the same as the one outlined here with an additional step for the diffusion of impulse since the evolution equation for impulse is Eq. (4). The forces have a tangential component as seen in Eq. (11) and thus the impulse vectors would no longer remain normal to the membrane. The diffusion process can be modeled by adding a random walk to the particle positions as is done frequently in vortex methods. However, since the boundary configuration is used to calculate forces, we anticipate that a deterministic method for the diffusion process will produce more satisfactory results.

ACKNOWLEDGMENTS

I thank my thesis advisor Professor Alexandre Chorin for many helpful suggestions. This work was supported in part by the Applied Mathematical Sciences subprogram of the Office of Energy Research, U.S. Department of Energy, under Contract DE-AC03-76SF00098; by the Air Force Office of Scientific Research AASERT Grant FDF49620-93-1-0053; and by the University of California Affirmative Action Dissertation-year Fellowship.

REFERENCES

1. C. Anderson and C. Greengard, *SIAM J. Numer. Anal.* **22,** 413 (1985).
2. G. R. Baker, *J. Fluid Mech.* **100,** 209 (1980).
3. G. R. Baker, D. I. Meiron, and S. A. Orszag, *J. Fluid Mech.* **123,** 477 (1982).
4. G. R. Baker, D. I. Meiron, and S. A. Orszag, *J. Sci. Comput.* **4,** 237 (1989).
5. G. K. Batchelor, *An Introduction to Fluid Dynamics* (Cambridge Univ. Press, New York, 1967).
6. J. T. Beale and A. J. Majda, *J. Comput. Phys.* **58,** 188 (1985).
7. T. F. Buttke, "Velicity Methods: Lagrangian Numerical Methods Which Preserve the Hamiltonian Structure of Incompressible Fluid Flow," in *Vortex Flows and Related Numerical Methods,* edited by J. T. Beale, G.-H. Cottet, and S. Huberson, NATO ASI Series C, Vol. 395 (Kluwer Academic, Dordrecht, 1993).
8. T. F. Buttke and A. J. Chorin, *Appl. Numer. Math.* **12,** 47 (1993).
9. A. J. Chorin, *Vortex Methods,* Les Houches Summer School of Theoretical Physics, Les Houches, France, 1993 (unpublished).
10. A. J. Chorin, *Vorticity and Turbulence* (Springer-Verlag, New York, 1994).
11. A. J. Chorin and J. E. Marsden, *A Mathematical Introduction to Fluid Mechanics* (Springer-Verlag, New York, 1979).
12. R. Cortez, Ph.D. thesis, University of California, Berkeley, 1995 (unpublished).

13. O. H. Hald, ''Convergence of Vortex Methods,'' in *Vortex Methods and Vortex Motion* edited by K. E. Gustafson and J. A. Sethian (SIAM, Philadelphia, 1991).
14. J. J. L. Higdon and C. Pozrikidis, *J. Fluid Mech.* **150,** 203 (1985).
15. J. D. Jackson, *Classical Electrodynamics* (Wiley, New York, 1975).
16. R. Krasny, ''Computation of Vortex Sheet Roll-up,'' in *Vortex Methods,* edited by C. Anderson and C. Greengard (Springer-Verlag, New York/Berlin, 1987).
17. P. Luchini, *AIAA J.* **29,** 474 (1991).
18. J. H. Maddocks and R. L. Pego, to appear, 1994.
19. M. F. McCracken and C. S. Peskin, *J. Comput. Phys.* **35,** 183 (1980).
20. R. Mendez, Ph.D. thesis, University of California, Berkeley, 1978 (unpublished).
21. V. I. Oseledets, *Commun. Moscow Math. Soc.* **44,** 210 (1989).
22. C. S. Peskin, *Mathematical Aspects of Heart Physiology,* Lecture notes, Courant Institute of Mathematical Sciences, 1975 (unpublished).
23. E. G. Puckett, ''A Review of Vortex Methods,'' in *Incompressible Computational Fluid Mechanics,* edited by R. Nicolaides and M. Ginzburger (Cambridge Univ. Press, Cambridge, 1992).
24. D. I. Pullin, *J. Fluid Mech.* **119,** 507 (1982).
25. P. H. Roberts, *Mathematica* **19,** 169 (1972).
26. P. Rouhi, manuscript, 1990 (unpublished).